J. Fluid Mech. (1981), *vol.* 111, *pp.* 59–85
Printed in Great Britain

Experimental study of physiological pulsatile flow in a curved tube

By K. B. CHANDRAN AND T. L. YEARWOOD

Hemodynamics Laboratory, Division of Materials Engineering and Center for Materials Research, College of Engineering, The University of Iowa, Iowa 52242

(Received 17 July 1979 and in revised form 8 January 1981)

In this paper, an experimental determination of the three-dimensional velocity distribution due to the physiological pulsatile flow of a Newtonian, incompressible fluid at various locations in a curved tube of circular cross-section is presented. Our results show four interesting features of the pulsatile flow development in the curved tube. First is the presence of a reversed flow along the inner wall of the tube during the diastolic (deceleration) phase of the pulsatile flow cycle. Second is that the flow does not appear to be fully developed in the curved tube through the cross-section whose L/a ratio is equal to 16·9, the final location at which measurements were made in this study, where L is the axial length and a is the radius of the curved tube. A third feature observed is the vacillation of the peak axial velocity across the horizontal diameter of the tube from the upstream to the downstream region in the curved tube. In the upstream region (L/a = 3·4), the maximum axial velocity measured occurred nearest to the outer wall. The maximum axial velocity shifted towards the inner wall in the middle of the tube (L/a = 10·2), while in the downstream region (L/a = 16·9), the maximum axial velocity measured was again near the outer wall. Finally, trapped vortical motions are observed to occur at the inner wall of the tube in the downstream region.

1. Introduction

In this paper, an experimental study of the three-dimensional velocity pattern due to the physiological pulsatile flow of a Newtonian incompressible fluid through a curved tube of circular cross-section is presented. The precise nature of the development of pulsatile flow in the entry region of a curved tube has relevance to the nature of flow in the human arterial system. The distribution of wall shear stresses in curved tubes and at bifurcations have been linked to atherogenesis as described in Bergel, Nerem & Schwartz (1976). Moreover, the nature of the development of secondary fluid motions in a curved tube during pulsatile flow is related to the study of fluid mixing in heat exchangers and blood oxygenerators.

Previous studies on steady and unsteady flows in curved tubes can be classified broadly in terms of fully developed flow and those in the entry region. A survey of literature of the previous studies is included in Yearwood (1979) and a brief review of the previous work pertinent to the present study follows.

The study of flow in curved conduits began with Boussinesq (1872) and was followed by Thompson (1879), whose studies grew out of an interest in the origin

of winding rivers and the erosion of river bends. His efforts were followed by Eustice (1911), Dean (1927, 1928) and others. Eustice completed the first conclusive experimental work on this problem, showing qualitatively the helical nature of the fully developed flows using dye filament studies.

The analytical solution to fully developed flow in curved tubes was given by Dean (1927, 1928), in which he found that the degree of the influence of curvature on steady streamlined flow is given by a non-dimensional parameter,

$$D = \left[\frac{U^2/R}{\nu^2/a^3}\right]^{\frac{1}{2}}, \tag{1}$$

where D is known as the Dean number, U is the average velocity, a is the tube radius, R is the tube centre-line radius of curvature and ν is the kinematic viscosity. This expression shows that D is the ratio of the effective centrifugal inertia forces to the viscous forces, in a fashion analogus to the Reynolds number. With increasing D, the effects of the centrifugal forces become stronger and greater secondary velocities would be expected to appear.

Dean's analytical solution to the equations of motion for this problem was qualitative and contained convergent results for the range of Dean numbers $0 \leqslant D \leqslant 96$. His solution was expanded upon by Barua (1963) for large values of D. Barua was able to derive an asymptotic boundary-layer solution to the equations of motion by assuming that the viscous forces at high Dean numbers are significant only in a thin boundary layer near the wall of the tube. Flows of moderate Dean numbers have been investigated numerically by McConalogue & Srivastava (1968) for the range of $96 \leqslant D \leqslant 605{\cdot}72$. A numerical analysis of the equations of motion for fully developed flows in curved tubes, covering a wide range of Dean numbers, has been performed by Truesdell (1963), Mori & Nakayama (1965), Sankaraiah & Rao (1973) and Greenspan (1973). Greenspan used a finite-difference algorithm to solve the equations of motion for a range of Dean numbers of $0 \leqslant D \leqslant 5000$. His results for secondary-flow velocities in the symmetric half plane show that as the Dean number increases, the core of the secondary flow progresses towards the inner wall of the tube. Conversely, the results for the axial flow, indicate that the axial momentum peak moves well away from the inner wall.

Assuming that laminar flow in a curved pipe will consist of a frictionless central core surrounded by a boundary layer, Ito (1969) used an approximate method of solution valid up to the immediate vicinity of the inside wall and compared his results with available experimental data. Collins & Dennis (1975) obtained numerical solutions for steady, fully developed flow in curved tube for range of Dean number between 96 and 5000. These two works showed that earlier numerical work of Greenspan suffered from inaccuracies especially at large Dean number.

Several studies have appeared recently in which unsteady fully developed viscous flows in curved tubes have been theoretically and experimentally investigated. Lyne (1971) and Zalosh & Nelson (1973) studied these flows in curved tubes produced by a sinusoidally varying pressure gradient. Lyne found that the secondary flows which resulted were governed by an unsteady Reynolds number, R_s, given by

$$R_s = \overline{W}^2 a/R\omega\nu, \tag{2}$$

where $\overline{W}$ is a typical velocity along the axis of the tube, ω is the frequency of the sinusoidal pressure gradient, and ν is the kinematic viscosity. For sufficiently large

values of ω, Lyne found that the flow could essentially be divided into two regions: (*a*) the core region, in which the flow is essentially inviscid and exhibits a secondary flow opposite in sense to that predicted for a steady pressure gradient; and (*b*) the boundary region, where viscous effects are dominant and exhibit secondary flows of the same sense as those predicted for a steady pressure gradient. Lyne reasons that centrifugal forces generate a secondary motion which is confined to a thin boundary layer at the wall (the Stokes layer). The fluid is caused to move along the wall circumferentially towards the inner wall, and then, returns towards the outer wall at the edge of the boundary layer. In doing so, it drags the fluid of the inviscid core region with it, giving rise to two regions of flow within the cross-section. The work of Zalosh & Nelson (1973) confirms these results. In a different study, Chandran *et al.* (1974) found similar results from a numerical analysis of oscillatory flow in thin walled curved elastic tubes, as a simulation of blood flow at arterial curvature sites. Through the use of a perturbation technique performed on a solution for oscillatory flow of a viscous fluid through thin-walled straight elastic tubes (Morgan & Kiely 1954), they showed that the secondary flow at the cross-section of the curved tube changed directions at various times during the period of oscillation. They also showed, as Lyne had shown earlier, that the maximum axial velocity shifted towards the centre of curvature of the tube and that the maximum wall shearing stresses occurred at the wall of the inner curve. Qualitative experimental verification of these numerical analyses was provided by Munson (1975). He used dye filament in a clear plastic circular tube formed into a hoop in which oscillatory flows of various frequencies were generated by a piston pump. For large values of frequency, he was able to show the two distinct flow regions as described by Lyne and Chandran *et al.* (1974). In looking at a different type of unsteady flow situation, Smith (1975) investigated the nature of viscous flow for an imposed pressure gradient of a pulsatile nature (sinusoidal with a non-zero mean) in rigid curved tubes of arbitrary but symmetric cross-section. His results are compatible with those found in the studies above. Chandran, Hosey, Ghista & Vayo (1979) have recently analysed fully developed, unsteady viscous flow in a thin-walled curved elastic tube. Using the same perturbation technique described earlier (Chandran *et al.* 1974), they computed the unsteady flow components of a physiologically relevant pulsatile flow pattern in a model of a thin-walled curved arterial segment and compared those results with the steady-flow velocity profiles obtained by Greenspan (1973) for Dean-number values up to 2350. Their results showed that the wall shear stress distribution over a cross-section of the tube was skewed considerably as a result of the steady component of the flow, the higher magnitudes of wall shear stress occurring at the outer wall of the bend. In contrast, however, superposition of the first six oscillatory modes to form the unsteady component of flow yielded wall shear stress of an order of magnitude greater than the steady flow component with higher wall shear stresses occurring at the inner wall of curvature. Furthermore, they found that the hoop stresses in the wall were several times higher than the corresponding axial stress values as a result of the unsteady flow components.

Steady entry flow in rigid curved tubes has been studied experimentally by Olson (1971), numerically by Patankar, Pratap & Spalding (1974) and analytically by Singh (1974) and Yao & Berger (1975). Agrawal, Talbot & Gong (1978) measured the axial and transverse velocity profiles experimentally for entry flow in a rigid curved

pipe with laser anemometry. They showed that the correlation between their experimental results and the theoretical work of Yao & Berger (1975) was poor, possibly because of erroneous assumptions used in their solution procedure. Their results also show that the boundary layer along the outer wall becomes thin, whereas the boundary layer along the inner wall of the curve thickens. These investigations have have all been concerned with tubes of a relatively small degree of curvature. Choi, Talbot & Cornet (1979) measured the wall shear rates due to steady entry flow in a curved tube by an electrochemical limiting current method and presented results for the distribution of wall shear both in the circumferential and axial directions. Their results suggested the existence of several pairs of vortices in a developing curved tube flow as opposed to a fully developed flow where only a single pair of vortices is observed.

Another recent experimental study was done by Scarton, Shah & Tsapogas (1977) on steady entry flow in a tube of severe curvature, having a tube radius-to-radius of curvature ratio of 0·312, which closely approximates the geometries of the human aortic arch. Using dye filament studies, they were able to visualize the development of the boundary layer along the inner and outer walls of the curved tube from an inviscid core region. From their results, they derive the following interpretation. At the entrance of the tube, fluid having a uniform entry velocity behaves as if it is inviscid, and the axial velocity at the inner wall is greater than at the outer wall. However, they reason, the thin outer wall boundary layer contains a very strong centripetally induced secondary flow which draws the slower moving fluid from the outer wall to the inner wall. At the inner wall, the fluid is trapped. When a typical streamline, which is moving axially in the direction of the tube centre-line, comes in contact with the growing boundary layer, it decelerates axially (because of the no-slip condition at the wall) and accelerates circumferentially along the wall towards the inner wall. Upon reaching the inner curve wall, the fluid attempts to re-inject into the high-speed potential core. Scarton *et al.* believe, however, that this injection cannot occur because of a lack of outward radial momentum. The fluid, therefore, returns to the wall of the inner curve where it becomes trapped in a counter-rotating fully developed Dean vortices.

Unsteady entry flow in rigid curved tubes has been studied by Pedley (1975, 1976) and Singh, Sinha & Aggarwal (1978). Pedley's unsteady analysis is based on an approximation theory developed to investigate boundary layers in reversing flows across a flat plate (Pedley 1974). However, he only attempted to predict the oscillations in shear rate as a function of axial distance from the entrance. The work of Singh *et al.* is an expansion upon the steady entry flow study of Singh (1974) using a boundary-layer analysis and examines the consequences of pulsatile flow (sinusoidal flow with a non-zero mean) in a rigid tube with a tube radius-to-radius of curvature ratio of 0·10. They indicate that the fluid velocity will initially be higher near the inner wall of the curved tube owing to geometric factors. However, as the flow develops, they predict that the effect of curvature will be to increase the secondary flow in the boundary layer, drawing fluid azimuthally from the outer wall to the inner wall. As the fluid is drawn towards the inner wall, the boundary layer there thickens while at the outer wall, the boundary layer becomes thinner. This implies that the wall shear at the outer wall will become greater than at the inner wall as the flow develops further downstream. Furthermore, for this location downstream, their

analysis predicts the gradual development of a reversed flow during the deceleration phase of the flow cycle near the inner wall, where the slower moving fluid responds readily to an adverse pressure gradient. Their analysis also shows that the displacement effect of the boundary layer on the core is not significant because, for this type of unsteady flow in a tube of slight curvature, the boundary layer remains thin, about one-tenth of the tube diameter.

In this paper, an experimental study of pulsatile entry flow in a curved tube of radius to radius of curvature ratio of 0·10 is reported. The axial, radial and tangential components of the velocity vector were measured using a three sensor hot-film probe at various cross-sections in the curved tube. This study is an extension on our previously reported work (Chandran, Yearwood & Wieting 1979) where we used the flow visualization technique to qualitatively describe the flow in the curved tube and a single probe to measure the axial velocity component. Due to the obvious physiological applications of this study, our experiments have been restricted to a pulsatile flow with a period of 72 Hz and a time-averaged flow rate of 5·2 l min^{-1} representative of a normal cardiac output in humans. Even though the radius to radius-of-curvature ratio in a human aorta is about 0·40, a curved tube with a ratio of 0·1 was deliberately chosen since it was felt that a tube with smaller curvature will not be dominated by the effects of developing secondary flows, and will therefore facilitate obtaining a meaningful interpretation of the results.

2. Experimental methods

An acrylic curved tube of constant diameter and circular cross-section which had a tube radius-to-radius of curvature ratio (ϵ) of 0·10 was fabricated for this study. This curved tube flow chamber was machined out of two halves of a Plexiglas sheet. A circular trough with a radius of 15 mm and a uniform radius of curvature of 150 mm was cut in each half through the use of an endmill and a rotary table. The halves were then highly polished and cemented together with silicone adhesive cement. Figure 1 shows a schematic diagram of this tube. The tube curved through an angle of 116·4°, and the planes in which measurements were to be taken were chosen at equal increments of 19·4° each from the tube entrance, as shown in figure 1. Holes were drilled on the top and side of the flow chamber at each plane upon completion of the flow visualization study (Chandran, Yearwood & Wieting 1979) to allow for the insertion of the velocity probe. These holes enabled the hot-film probe to make a horizontal (in the plane of the curvature) and vertical (perpendicular to the plane of curvature) traverses in the tube. Each hole was a $\frac{1}{2}$-inch NPT threaded hole which was carefully centred with respect to the geometry of the tube at each recording station. Table 1 gives the angle θ, the axial distance L, and the axial distance to radius ratio (L/a) for each of the five planes, A–E, where measurements were made in the tube. The acrylic curved tube was incorporated into a mock-circulatory system providing physiological pulsatile flow of blood analog fluid into the experimental flow chamber. The schematic diagram of the mock-circulatory system is shown in figure 2 and the details of the components of the system are included in Yearwood (1979). In the interest of brevity, only the salient features of the flow system are described below. The pneumatic pulser provides a silicone rubber diaphragm pump with compressed air driving it against the fluid of the flow system.

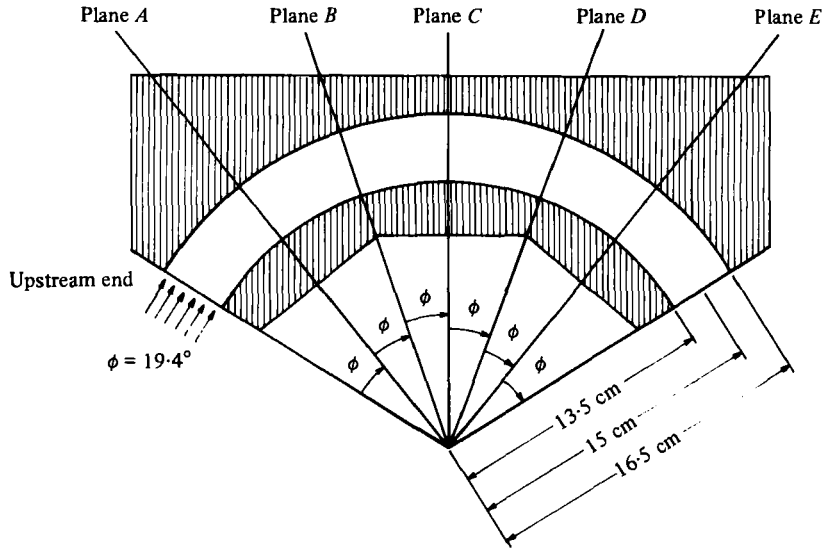

FIGURE 1. Schematic diagram of the curved tube used in these experiments, indicating the planes at which velocity measurements were obtained.

Plane	*Angle from entrance*	*Axial distance, L* (mm)	*L/a*
A	$\theta = 19{\cdot}4°$	50·9	3·39
B	38·8°	100·1	6·67
C	58·2°	152·4	10·16
D	77·6°	203·1	13·54
E	97·0°	254·0	16·93

TABLE 1. Geometrical data for the curved tube; $\epsilon = 0{\cdot}10$, Tube radius $a = 15$ mm, radius of curvature $R = 150$ mm.

Under the operating conditions for the experiment, the pulse rate of the pneumatic pulser was adjusted to 72 pulses per minute (834 ms per cycle) with a systolic duration of 270 ms. The driving pressures needed to produce a mean flow rate of 5·2 l min^{-1} through the mock-circulatory system were 135 mmHg with a concomitant vacuum of approximately 8 mmHg below atmospheric pressure.

A Gott butterfly leaflet aortic valve was mounted in the aortic valve chamber (figure 2) for these experiments. Since a uniform entry flow profile was desired at the entrance to the curved tube, the downstream aortic valve chamber was replaced by a flow straightener. This flow-straightening section was designed to minimize the disturbances created by the valve prosthesis, thus allowing the study of pulsatile laminar flow of uniform entry through the curved tube. The Gott butterfly leaflet valve was chosen for these experiments for two reasons. It has an unusually small degree of fluid back flow during the diastolic portion of the cardiac cycle. Moreover, the fluid disturbances generated by the Gott valve contained relatively little secondary vortices and these could be effectively dampened by the flow-straightening section described above (Wieting 1969). As observed from our flow-visualization studies (Chandran, Yearwood & Wieting 1979), vortex shedding at the tips of the two leaflets of the Gott valve had completely dissipated by the end of the flow

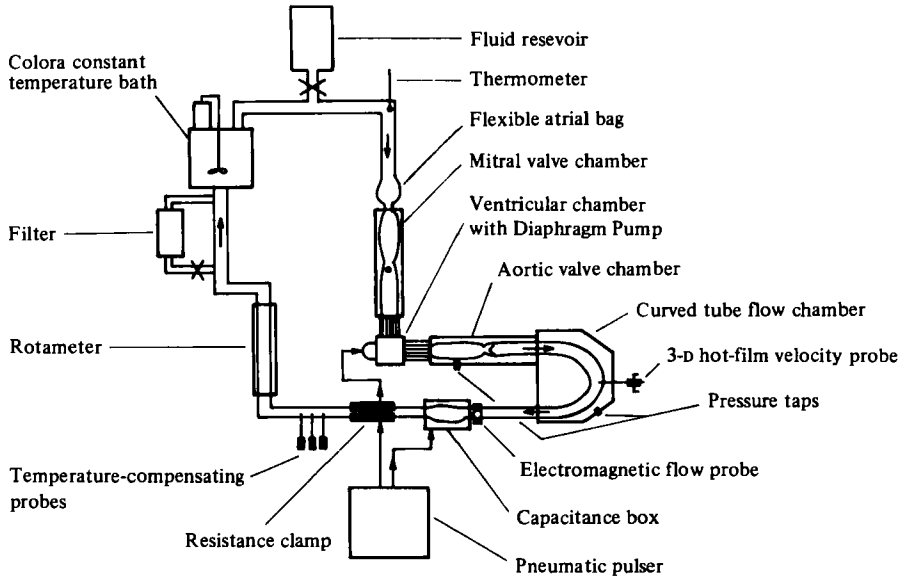

FIGURE 2. Schematic diagram of the pulsatile flow system.

straightener. Figure 3 shows the instantaneous flow rate at the exit of the curved tube as recorded by electromagnetic flowmeter. The peak flow at systole, as seen in this figure, is 18·3 l min^{-1}. In addition, immediately after the valve closure, very little forward flow and virtually no reversed flow is observed from the flowmeter recording.

The fluid used in the experiment was an aqueous glycerol solution consisting of 42·6% glycerine by volume. The viscosity of this solution was measured in the laboratory to be 4·46 cps at 37 °C (the temperature maintained throughout these experiments) and the specific gravity was measured to be 1·133. The pressure pulses upstream to the aortic valve as well as in the curved tube were monitored by Statham pressure transducers using fluid-filled catheters. The flow rate signal from the electromagnetic flowmeter as well as the pressure pulses were maintained to be the same throughout the sequence.

The three-dimensional hot-film anemometer velocity probe used in these experiments was a three-sensor probe manufactured by Thermo-Systems, Inc. (Model no. 1298), as shown schematically in figure 4. This probe was operated by three constant-temperature anemometers (TSI, Model 1050), one for each sensor of the probe. Each sensor has a diameter of 0·4 mm and a length of 2 mm, and their centres are spaced 0·5 mm apart. It was temperature compensated by three temperature compensating probes (TSI Model no. 1310 with the associated TSI Model no. 1325 Trimming Networks), even though the fluid was maintained at $37 \pm 0{\cdot}2$ °C by the constant-temperature bath. The orientation of the three sensors of the probe with respect to the mean flow direction is shown in figure 4. The calibration of this three-sensor probe is described in detail in Yearwood (1979).

An AMPEX FR1300 FM magnetic recorder was used to record the anemometer signals, as well as flow signals from the Carolina Electromagnetic Flowmeter and the triggering circuit attached to the pneumatic pulser. Flow signals originating from

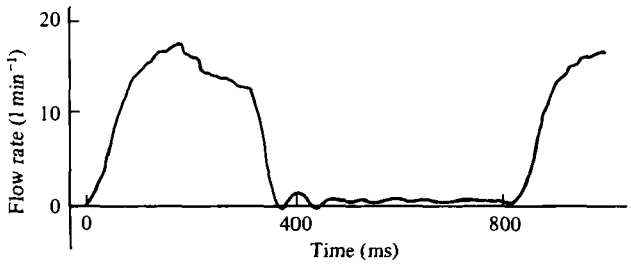

FIGURE 3. The flow rate versus time curve, obtained by an electromagnetic flow probe downstream to the curved tube. The aortic value mounted upstream to the flow straightener was a Gott butterfly prosthesis.

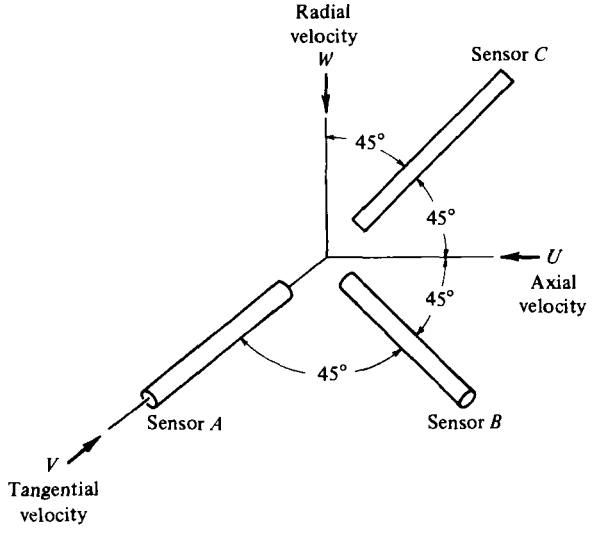

FIGURE 4. Schematic diagram of the three-dimensional hot-film velocity probe showing the configuration of the sensors to the components of the total velocity vector.

the electromagnetic flow probe placed near the exit of the experimental flow chamber were recorded after each successive set of anemometer recordings at a particular site within the flow chambers. The pneumatic pulser provided a square-wave trigger signal through a triggering circuit near the beginning of each cardiac cycle. This trigger signal was recorded simultaneously with the signals from the anemometers and then with the signals from the flowmeter. In this way, anemometry data at a given site in the flow chamber could be accurately related in time to data collected at other locations along the same traverse and throughout the flow chamber.

Analog data were collected from the three-sensor hot-film probe in the experimental flow chamber in the following manner. The probe was successively inserted through the $\frac{1}{4}$-inch holes drilled into the top and sides of the flow chamber at five stations, planes *A*–*E* as shown in figure 1. The tip of the probe was carefully aligned with the wall of the chamber for both the horizontal and vertical traces across each plane, and the body of the probe was oriented with the major axis of the chamber so that it faced the oncoming flow. The outputs of the three anemometers were then recorded on magnetic tapes for a series of cardiac cycles. The probe was then rotated

180° so that it faced flow in the reverse direction, and the anemometer outputs for similar number of cardiac cycles were recorded on magnetic tape. It was then moved to the next point of data collection with the aid of calipers, and recordings were again made for both forward flow and reversed flow directions. Data were collected at every 2 mm across the diameter for both horizontal and vertical traverses at each cross-section. The analog data from the anemometers and the electromagnetic flowmeter were ultimately digitized and averaged. Each sweep of the signal averager was initiated by the recorded trigger signal, and had a duration of 1·23 pulsatile flow cycles. Examples of the raw analog data from the anemometer pulses in comparison with wave forms produced from the digital averages of 16 sweeps across are shown in figure 5. This figure shows the raw data in comparison with the averaged wave forms produced by a series of averaging tests. In each successive test, an increasing number of sweeps of the cardiac cycles were averaged together as shown. Note that the wave form produced by only 16 sweeps is substantially smoother than its predecessors, whereas, the wave forms produced by greater numbers of sweeps do not significantly improve upon the quality of this averaged wave form. It was, therefore, decided to average only 16 sweeps of the incoming data for each channel at each site in the model curved tube. In addition, the resolution of these averaged wave forms ensured that fluctuating components of the velocity vector at frequencies of up to 2 kHz could be accurately digitized and averaged. For example, the sharp spike in the velocity wave form corresponding to the closing of the aortic valve is readily apparent even in the wave form produced by averaging 64 sweeps together as shown by the arrow in figure 5.

The digitized and averaged data obtained for these pulsatile flows was ultimately processed by a digital computer. In this step, the digital values for the nonlinearized bridge voltage data were linearized by an appropriate polynomial of order 7 or 8, obtained earlier by a least-squares regression analysis of the velocity calibration data for each sensor. These linearized bridge voltage values were then use to solve simultaneously the three equations

$$\left.\begin{aligned} E_A &= S_{AU}U - S_{AV}V + S_{AW}W, \\ E_B &= S_{BU}U - S_{BV}V + S_{BW}W, \\ E_C &= S_{CU}U + S_{CV}V - S_{CW}W. \end{aligned}\right\} \tag{3}$$

In these equations, E_A, E_B and E_C are the linearized bridge voltage outputs for sensors A, B and C, respectively, and U, V and W are the three components of the velocity vector in the x, y and z directions as shown in figure 4. S_{AV}, ..., S_{CW} represent proportionality constants of a given sensor to a change in the full bridge voltage output of that sensor as a result of a change in the local fluid velocity across it. These constants were previously obtained by the calibration procedure described in Yearwood (1979). By the simultaneous solution of the three equations, the radial, tangential and axial components of the local fluid velocity were obtained.

During a pulsatile flow cycle, 21 digital values evenly spaced in time from the initiation of the trigger pulse were processed for each location in the flow chamber. Figure 6 shows the approximate times on the averaged bridge voltage wave forms from planes A–E corresponding to these 21 samples.

Because hot-film anemometry is unable to differentiate between forward and

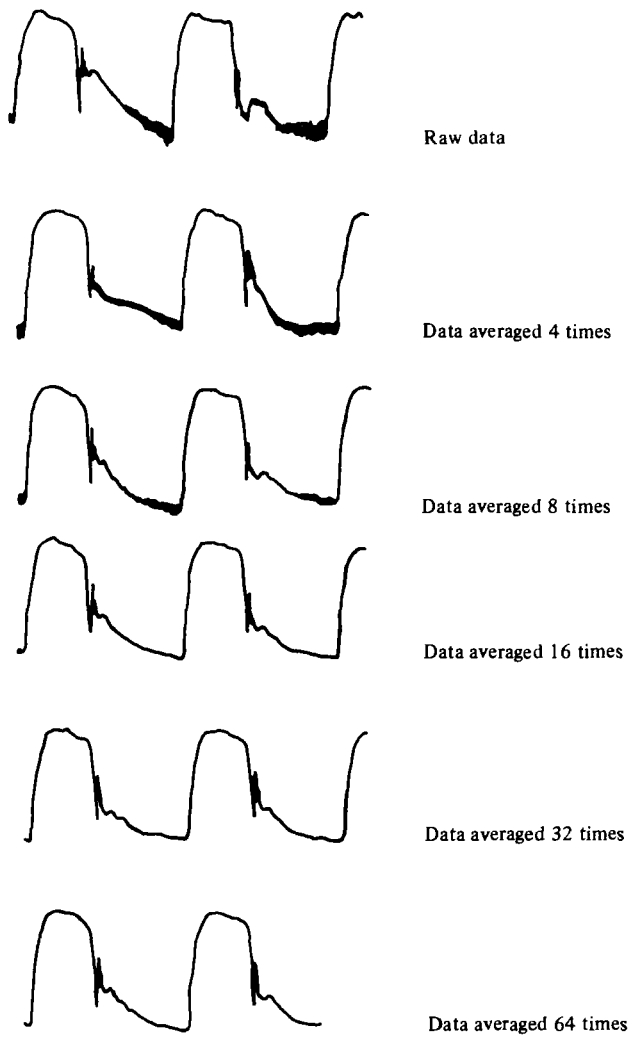

FIGURE 5. Bridge voltage output signals for successive cardiac cycles, obtained by sensor A of the hot-film velocity probe, and averaged by the Nicolet 1070 signal averager. Note that averaging more than 16 successive incoming bridge voltage signals does not significantly improve the resolution of the data.

reverse flows, the previous flow visualization studies played a significant role in the interpretation of the hot-film data. A direct correlation was observed between flow reversals as observed from the flow-visualization studies and the characteristics of the recorded anemometer signals as discussed below.

Figure 7 shows the averaged bridge voltage output versus time for sensor A. Sensor A was oriented perpendicular to the axial flow and was, therefore, sensitive primarily to changes in the axial velocity. The averaged wave form obtained from sensor A for various locations across the horizontal traverse is shown in this figure. These wave forms were produced by an $X-Y$ plotter which was linked directly with the Signal Averager. The wave forms are the results of plotting 4096 digital values across the allotted time span. At 2 mm from the inner wall, the resulting wave form

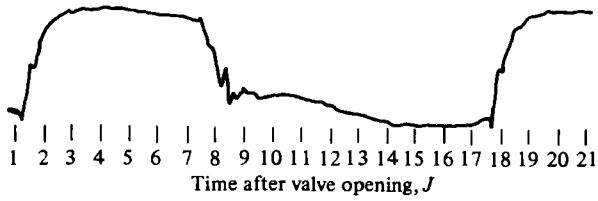

FIGURE 6. A typical bridge voltage output signal shown with respect to time from a location in the curved tube. The wave form comprises 1·229 cardiac cycles, over which 4096 data addresses (in time) were obtained and digitally averaged by the Nicolet 1070. The 21 arbitrarily chosen times, J, are shown here referenced to the opening of the prosthetic heart valve.

J = 1...−28·3 ms	J = 8...331·8 ms	J = 15...691·9 ms
2...23·1	9...383·2	16...743·3
3...74·6	10...434·7	17...794·8
4...126·0	11...486·1	18...846·2
5...177·5	12...537·6	19...897·6
6...228·9	13...589·0	20...949·1
7...280·4	14...640·4	21...1000·5

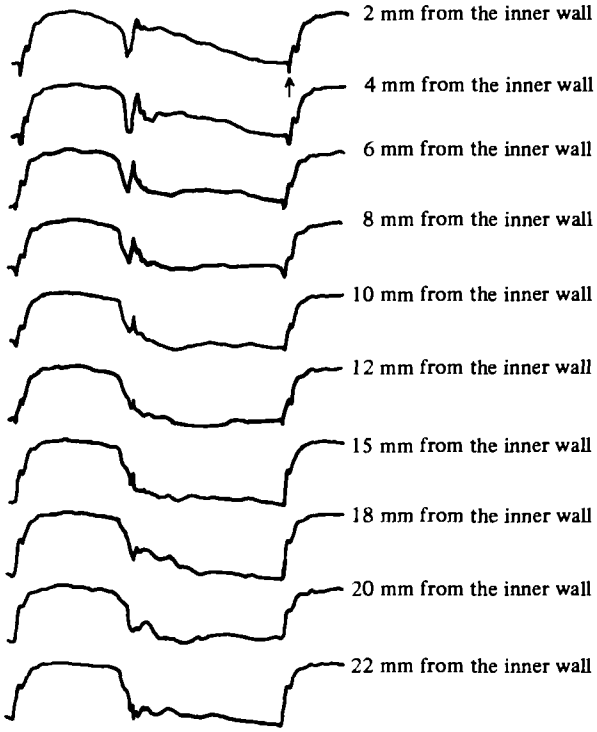

FIGURE 7. Averaged bridge voltage wave forms, with respect to time, for 1·229 cardiac cycles. Plane A, horizontal traverse.

is substantially different from that obtained near the outer wall at 28 mm from the inner wall. A particularly striking difference between these two wave forms is the character of the averaged signal during diastole. As indicated by the arrow in the wave form obtained at 2 mm from the inner wall, a noticeably sharp dip occurs at the end of diastole. Such a dip is not seen in the averaged signal obtained at 22 mm

from the inner wall. From our flow-visualization study, it is known that the flow along the inner wall is reversed during diastole (immediately after valve closure). At the beginning of the next cycle, the flow in that region has to reverse again towards the upstream direction and such a rapid flow reversal was indicated by the characteristic dip in the bridge voltage. On the other hand, in signals from near the outer wall region, where there was no reversed flow throughout the cycle, the dip in the bridge voltage was not observed. As seen in figure 7, at increasing distances from the inner wall, this characteristic dip in the wave form disappears. To see how this 'dip' enhances interpretation of the hot-film data, consider the following wave form. At 10 mm from the inner wall, the magnitude of the bridge voltage output initially decreases after valve closure. (Valve closure is always indicated by the characteristic spike in the bridge voltage output immediately after the period of systole.) Shortly after diastole begins, however, this very low bridge voltage output is seen to slowly rise, forming a slight 'hump' in the middle of the diastolic phase. It then exhibits a rapid dip in the wave form again at the onset of systole. A careful inspection of the high-speed ciné film data for this plane revealed that flow reversal slowly spread out across the horizontal traverse of plane A, decreasing in magnitude as it did so, and that at 10 mm from the inner wall, axial flow was reversed later in diastole compared with that at 2 mm from the inner wall. By carefully comparing the average bridge voltage output for other data sites in the curved tube, it was eventually possible to link the data provided by these wave forms to that obtained from the flow-visualization study to pinpoint locations within the tube where reversed flow did or did not occur during diastole. This proved to be a valuable technique in interpreting the velocities ultimately computed from the bridge voltage data.

3. Results and discussion

The geometric and material property data used in the experiment together with the values of dimensionless parameters are given in table 2.

The magnitude of the velocity at the inlet of the curved tube in the flow straightener was not directly measured so as to avoid drilling holes in the flow straightener and thus introducing another source of possible flow disturbance before the fluid enters the curved tube. However, velocity measurements were made in another tube with the same geometry as the flow straightener at the same axial distance away from the valve and the velocity distributions at early and peak systole (10 ms and 67 ms after the opening of the valve) are shown in figure 8. The velocity distribution was observed to be symmetric with respect to the centre of the tube, reasonably flat at the point of entry into the curved tube with a variation of less than 10 % between maximum and minimum magnitudes during peak systole.

The results of the measured velocity profiles for both horizontal and vertical traverses of planes A–E in the curved tube are presented below. Details of the axial, radial and tangential velocity components as computed from the signals recorded from the three-sensor probe at various times during a pulsatile flow cycle are presented for planes B and E. A comparison of the axial velocity components at various planes at a given time in systole and diastole is also presented subsequently.

The axial, radial and tangential velocity components for both horizontal and vertical traverses are included in figures 9 and 10, respectively. The axial velocity

Density of the fluid, $\rho = 1{\cdot}13$ g cm^{-3} at 37 °C
Viscosity coefficient, $\mu = 0{\cdot}45$ g cm^{-1} s^{-1}.
Frequency of the pulsatile fllow cycle, $\omega = 72$ cycles min^{-1}.
Radius of the curved tube, $a = 1{\cdot}5$ cm.
Radius of curvature, $R = 15{\cdot}0$ cm.
$\alpha = a\,(\omega\rho/\mu)^{\frac{1}{2}} = 20{\cdot}76$.

	Cross-sectional averaged velocity ($V = Q/A$)	Reynolds number ($Re = \rho Vd/\mu$)	Dean number ($D = Re(a/R)^{\frac{1}{2}}$)
Peak value during cycle	42·4 cm s^{-1}	3300	1140
Mean value over a cycle	12·0 cm s^{-1}	1020	320

TABLE 2

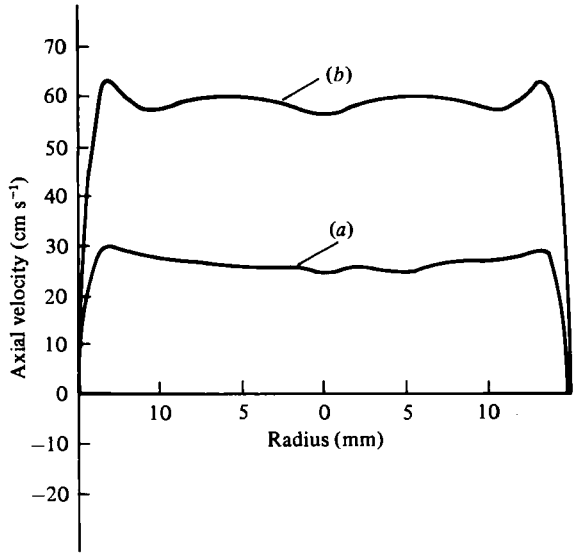

FIGURE 8. Velocity profile at the inlet of the curved tube. (*a*) Early systole (10 ms). (*b*) Peak systole (67 ms).

profiles for both horizontal and vertical traverses across the tube are relatively flat during systole ($J = 2$, 6). This flat velocity profile in the horizontal traverse is in contrast to the one seen for plane A during systole (Yearwood 1979, see also figure 13) where the axial velocity profile is skewed towards the outer wall. During diastole ($J = 10$), the flow along the inner wall is seen to be reversed (figure 9).

With the progression of diastole ($J = 12$, 17), the region of reversed flow extends towards the centre of the tube. The peak reversed flow at $J = 10$ is 25 cm s^{-1}, at $J = 12$, it is 19 cm s^{-1} and by $J = 17$, it has dropped to 10 cm s^{-1}. Reversed axial velocity is not observed in the vertical traverse until late in diastole ($J = 17$) and the region of reversed flow is confined to the centre of the tube. Since the horizontal and vertical traverses bisect each other at the centre of the tube, the flow reversal observed in the central region of the vertical traverse during late diastole, corresponds with the flow reversal observed in this region in the horizontal traverse.

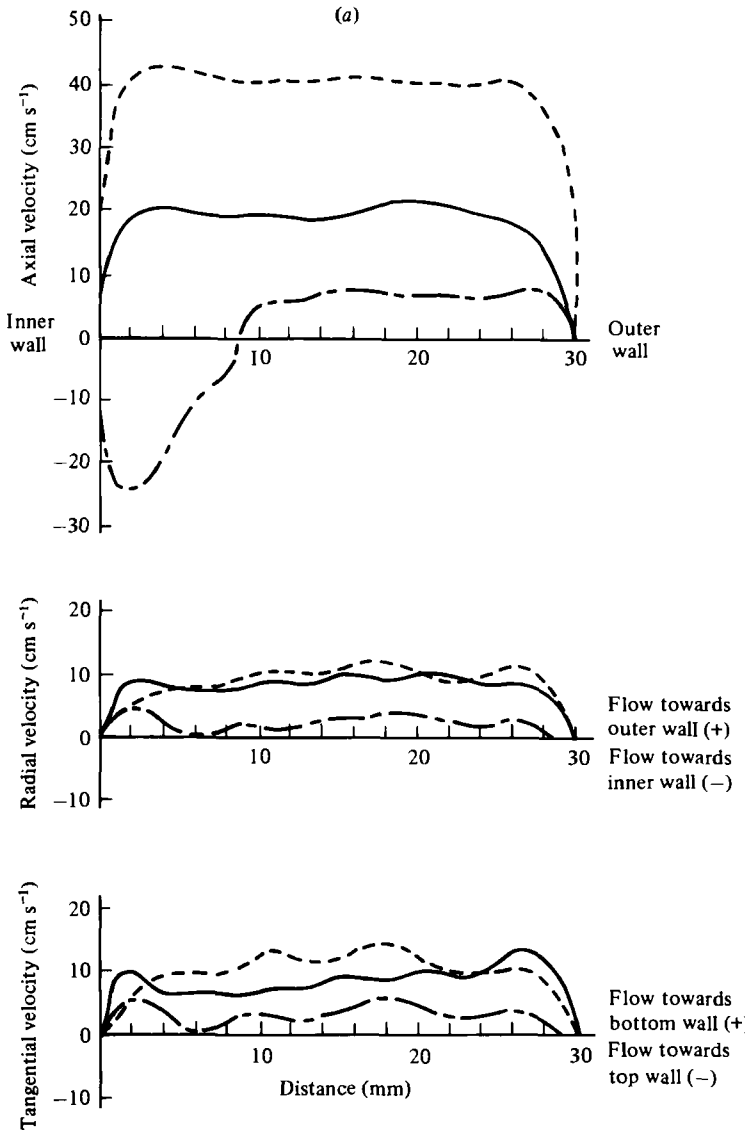

FIGURE 9(*a*). For caption see p. 73.

The radial and tangential velocity components are relatively flat during systole, except near the walls indicating the spatial dimension of the developing boundary layer at these locations. During early diastole, when the axial velocity is reversed near the inner wall, both the radial and tangential velocity components decrease in magnitude near the crossover point along the tube diameter between the forward and reversed flow regions. From the secondary velocity components, it can be seen that the flow in the core region is directed towards the outer wall as a result of the outward momentum gained in passing over the reversed flow regions of the curved tube in early systole. This produces a concomitant flow along the top and bottom walls towards the inner wall at planes *A* and *B*. Because the flow regime is a developing one, the stream lines of these secondary flows need not be closed (Agrawal *et al.*

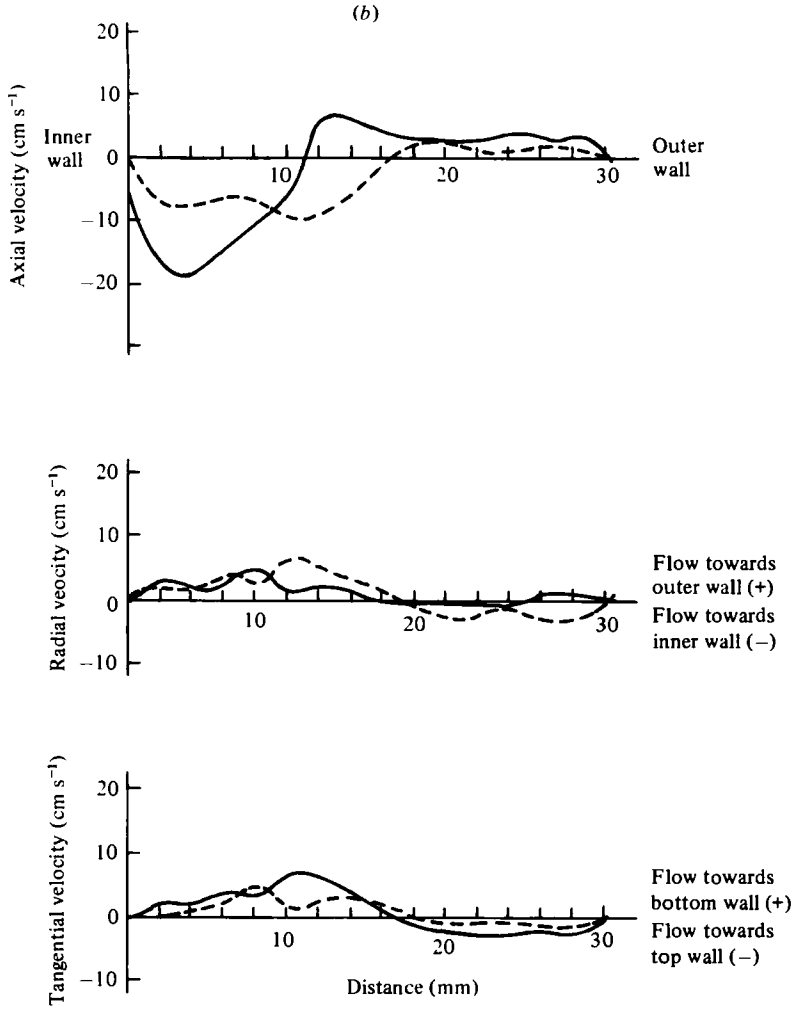

FIGURE 9. Axial, radial and tangential velocity profiles for plane B, horizontal traverse. (a) ——, $J = 2$; - - -, $J = 6$; — · —, $J = 10$. (b) ——, $J = 12$; - - -, $J = 17$.

1978). The high axial flow at the outer wall of plane A with its outwardly directed momentum has pushed against the wall of the tube and is returning towards the inner wall circumferentially above and below the core region.

The secondary flows also exhibit a tendency to move towards the bottom wall as observed from the secondary velocity profiles as well as slightly higher magnitudes near the bottom wall of the axial velocity profiles in the vertical traverse. As discussed by Yearwood (1979), this tendency is the result of the flow over the Gott butterfly valve leaflets not being symmetric.

With the progression of diastole ($J = 12, 17$), the radial velocity for the horizontal traverse is directed towards the outer wall, and this outward momentum explains the progressive reversal of the axial flow into the central core region. The magnitudes of the radial and tangential velocity components are relatively small in the horizontal traverse during this period since the outward momentum as the result of the centrifugal force dies out after valve closure and the cessation of a rapid forward flow in the tube.

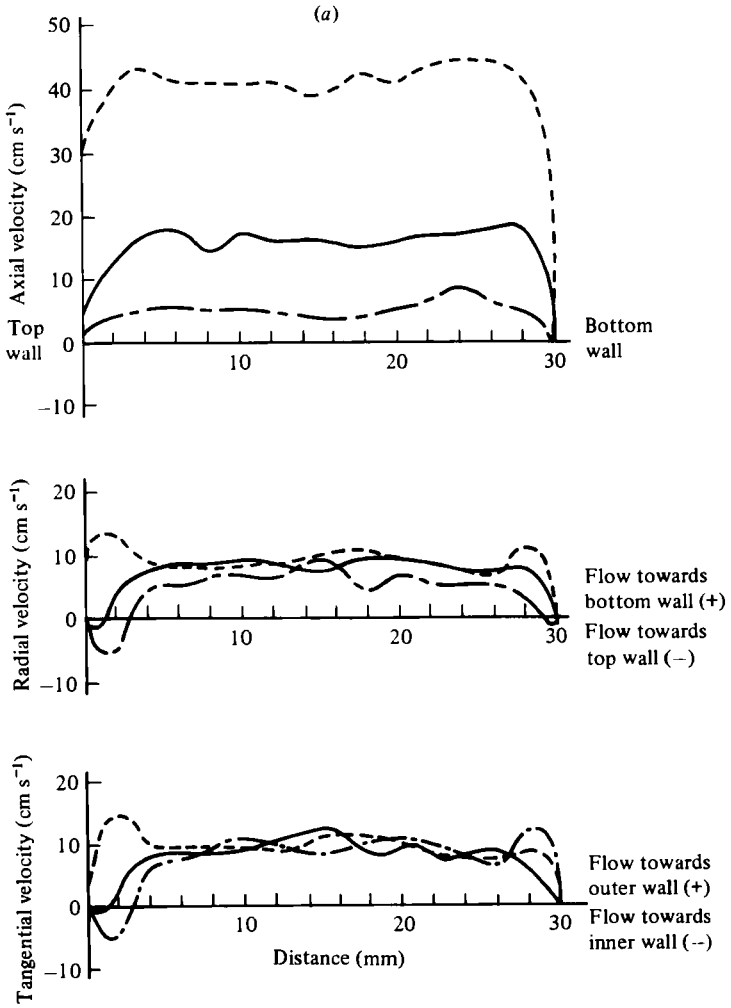

FIGURE 10 (*a*). For caption see p. 75.

The velocity components for horizontal and vertical traverses for plane E are presented in figures 11 and 12. The predominant feature of the axial velocity profiles across the horizontal diameter at $J = 2$ and $J = 6$ are the asymmetrical peak velocity measurements at the outer wall and the dramatic decrease in magnitude at 6 mm from the inner wall. The reversed flow along the inner wall of the tube at $J = 10$, $J = 15$ and $J = 17$ increases progressively toward the central region throughout diastole, while the forward flow at the outer wall remains much greater than at previous planes. Therefore, when the forward flow of systole encounters this residual reverse flow in the centre of the tube, the momentum of fluid in the centre of the tube is reversed producing a strong rise in the outwardly directed radial flow of the outer wall boundary layer for $J = 2$ and $J = 6$ in figure 12.

The notch that develops in the axial velocity near the inner wall of plane E during systole is the result of the onset of vortical motions within the boundary layer of the inner wall. The radial and tangential flow profiles shown in figure 12 decrease strongly at the border of the inner wall boundary layer and the core flow of the

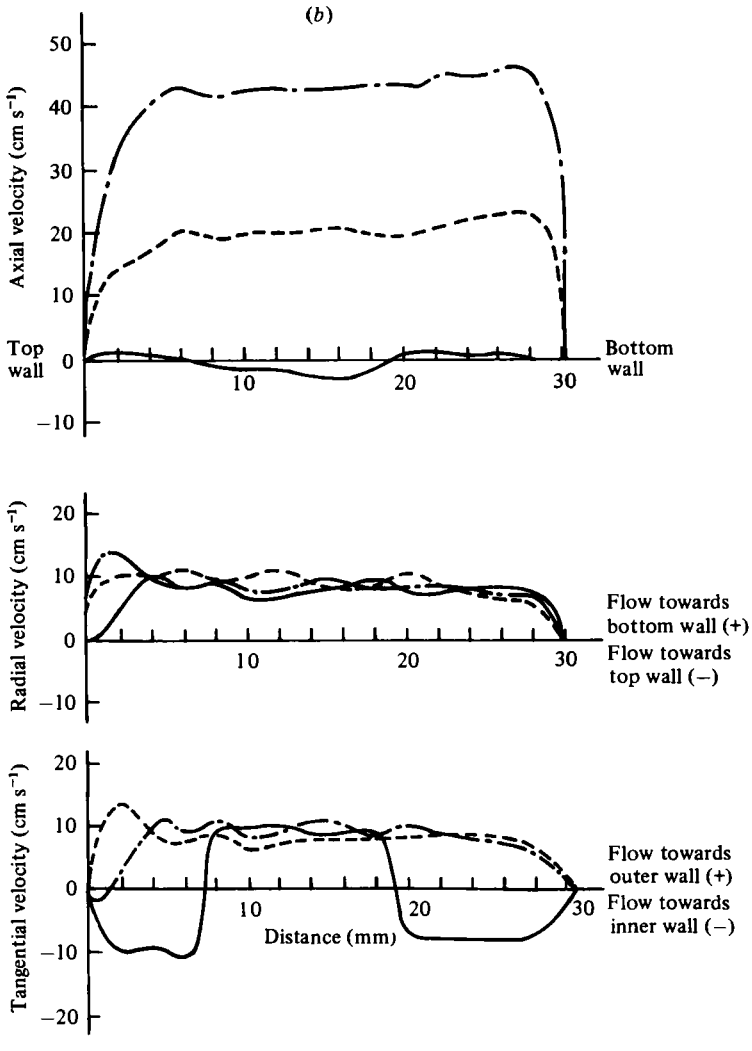

FIGURE 10. Axial, radial and tangential velocity profiles for plane B, vertical traverse. (a) ——, $J = 2$; — - —, $J = 6$; —·—, $J = 10$. (b) ——, $J = 12$; – – –, $J = 17$; —·—, $J = 19$.

central region of the tube. Tangential and radial flows in the boundary layer of the inner wall are great enough to enhance rotational motions within the boundary layer, and it is postulated that during systole, Dean's vortices develop within this boundary layer in a manner similar to that described by Scarton *et al.* (1977) for steady flow. The origins of these vortical motions are to be found in planes B and C, where inwardly directed circumferential motions during systole are measured along the vertical traverse across the tube diameter, thus feeding the boundary layer of the inner wall with fluid containing rotational momentum. By plane E, it is likely that any rotational flows entering the boundary layer of the inner wall at planes B and C, are therefore, unable to re-enter the potential core due to a lack of sufficient radial momentum. This lack of radial momentum is shown in figure 13 by the decrease in outward radial velocity at 6 mm from the inner wall. As a result, these isolated rotational motions become trapped Dean's vortices at plane E.

During diastole, a very strong reversed flow occurs at the inner wall which is broader and initially more extended than the reversed flow seen at plane D for the same stage of the cardiac cycle. Secondary motions across the horizontal plane decrease substantially in magnitude over the course of the diastolic phase as seen in figure 11 for the region of plane E. The attrition between forward flow at the outer wall and the reversed flow extending into the centre of the tube generate regions of relative stasis. Because of these very low velocities during diastole, it is unlikely that rotational motions in the boundary layer of the inner wall are generated during this phase of the cardiac cycle. An inspection of the axial velocity profile as it develops from $J = 17$ to $J = 2$, and then, to $J = 6$ in figure 12 will confirm that the evolution of vortical motions in the boundary layer of the inner wall is uniquely a function of flows generated during systole at locations upstream of plane E.

A superposition plot of the axial velocity components at planes A, C and E at $J = 6$ (during systole) and $J = 10$ (at the beginning of diastole) for the horizontal traverse are shown in figures 13 and 14, respectively. In these figures, the profiles from planes B and D are eliminated so as to avoid making the figure too cumbersome. At systole, in plane A, the maximum axial velocity is observed near the outer wall. This profile is in contrast to that observed in the entrance region of the curved tube for steady flow (Scarton *et al.* 1977; Agrawal *et al.* 1978). In the case of steady flow, the fluid in the potential core at the entrance region exhibits a profile skewed towards the inner wall, before both the viscous effects and the centrifugal forces reshape the axial velocity profile towards the outer wall across the plane of curvature in the downstream region. In contrast, in the case of pulsatile flow, as the flow in the tube accelerates at the onset of a new cycle it encounters reversed flow along the inner wall and the forward axial momentum is impeded. At the outer wall region, the residual forward axial momentum is enhanced by the rapid acceleration and the net effect is the skewing of the axial velocity profile towards the outer wall. As discussed earlier, at plane B the axial velocity profile is relatively flat compared to that of plane A and by plane C the axial velocity has a maximum near the inner wall. This effect is due to the onset of secondary flows between planes A and C as discussed earlier in detail for plane B. The outward-directed secondary flow at plane A is returning circumferentially along the top and bottom walls to the inner wall region and hence the outward skewing of the axial velocity disappears at plane B. At plane C this effect is manifested by a higher axial velocity near the inner wall. Between planes C and E, the axial velocity profile undergoes another transition and the profile is once again skewed towards the outer wall. As discussed earlier, the fluid fed into the inner wall boundary-layer region at plane C owing to the secondary flows appears to be trapped in the boundary-layer region as Dean's vortices and hence, the resulting notch in the axial velocity profile at 6 mm from the inner wall. Away from the boundary layer, the rapid flow acceleration with the onset of a new cycle is enhanced along the outer wall region and impeded towards the inner wall region due to the reversed flow from the previous cycle and hence, the profile is once again skewed towards the outer wall.

The axial velocity profiles for planes A, C and E along the horizontal traverse in figure 14 shows the flow reversal at the onset of diastole (immediately after the valve closure) along the inner wall of the curved tube. As seen in the figure, the flow reversal at plane E extends more into the central region compared to planes A and C

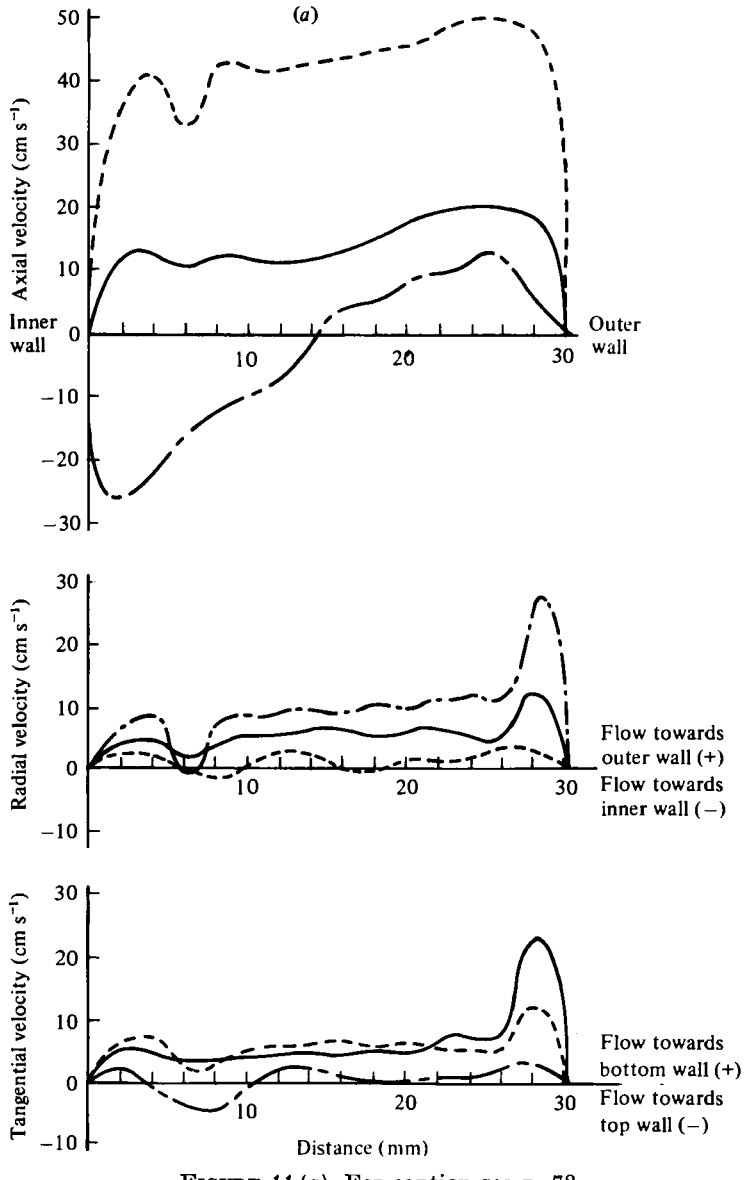

FIGURE 11 (*a*). For caption see p. 78.

even this early in diastole. As shown earlier for planes B and E, with the progression of diastole, the flow reversal extends towards the central core region for all planes even though the magnitude of the reversed flow velocity decreases.

The profiles shown in figures 15 and 16 for $J = 6$ and $J = 10$, respectively, along the vertical traverse appear to be relatively flat in all the planes. However, for planes A and C in figure 15 ($J = 6$), a noticeable dip is observed near the bottom wall. Since the Gott aortic valve prosthesis was oriented horizontally during these experiments, these velocity profiles suggest that the flow over the valve leaflets was not entirely symmetric. The valve was purposefully oriented in this horizontal position to avoid confusing the effects of curvature with artifacts produced by the

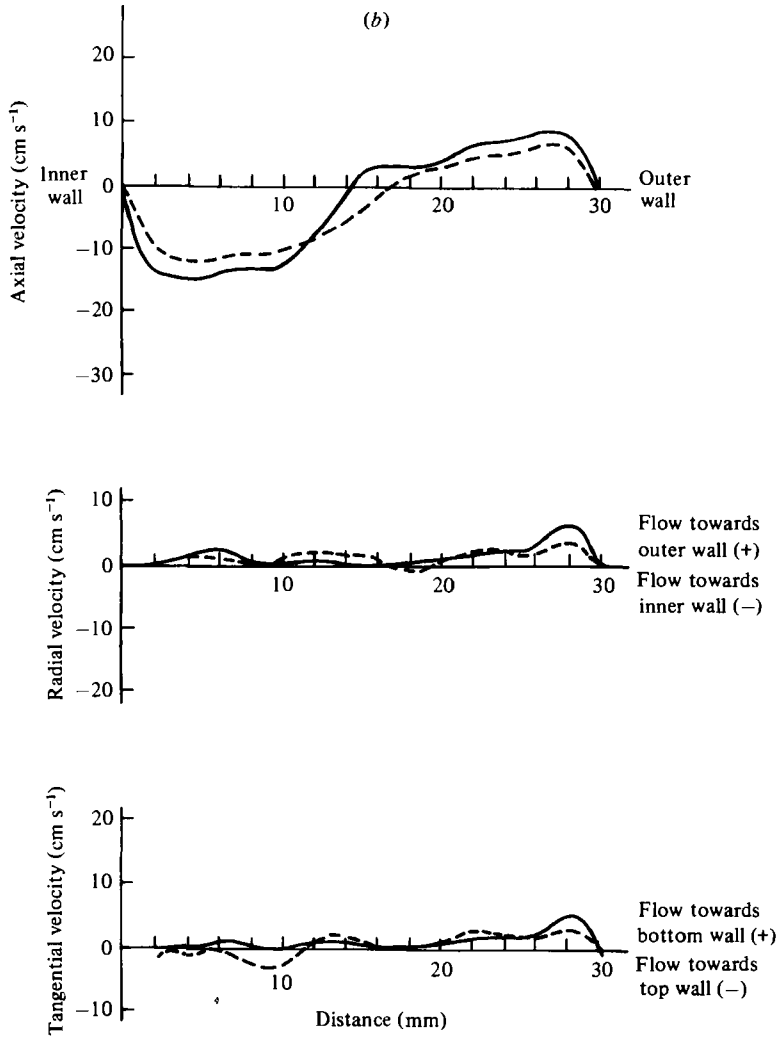

FIGURE 11. Axial, radial and tangential velocity profiles for plane E, horizontal traverse. (a) ——, $J = 2$; – – –, $J = 6$; — · —, $J = 10$. (b) ——, $J = 15$; – – –, $J = 17$.

disproportionate stiffness to the two leaflets. $J = 10$ represents the beginning of diastole and no flow reversal is observed either in the top or bottom wall. As discussed earlier for plane B, only towards the end of the diastole will a slight flow reversal be observed in the central region of the tube along the vertical traverse. This, of course, corresponds to the flow reversal extending to the central region of the tube towards late diastole.

Figures 17 and 18 represent an estimation of the fluid shear stress and shear rate at the walls of the tube as determined by a first-order finite-difference approximation applied to the axial velocity profiles in the tube. These values are only approximate due to two reasons. Firstly, as pointed out by Choi *et al.* (1979), this method of estimating shear stress is inaccurate and a direct determination of the shear stress as employed in their work should yield more accurate results. Secondly, we have also

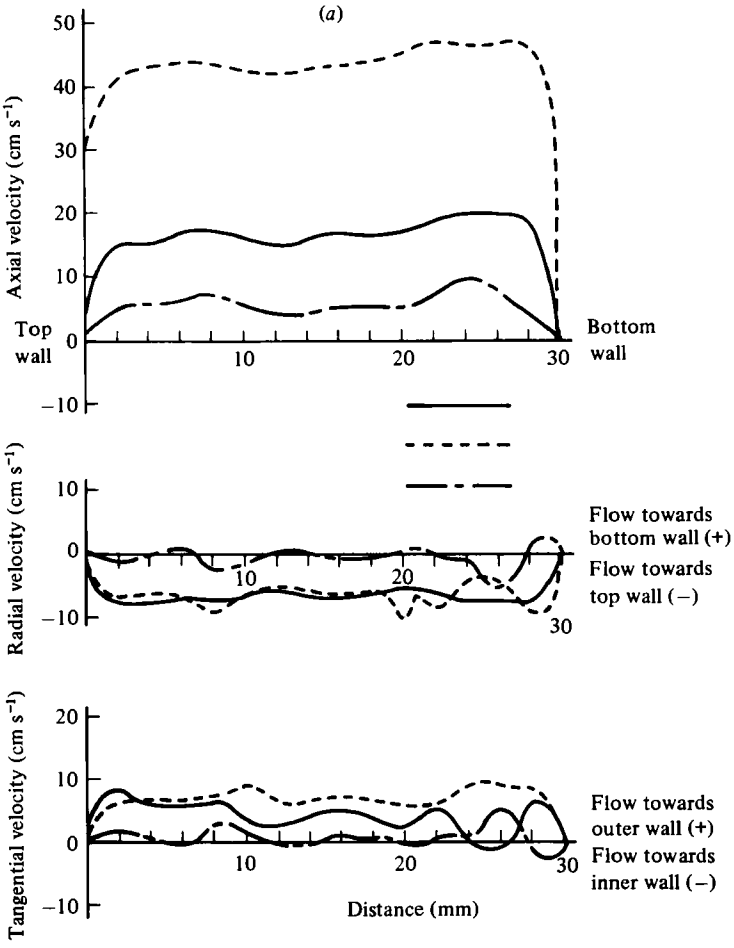

FIGURE 12(*a*). For caption see p. 80.

not taken the transverse component of the shear stress in our computation. However, these *approximate* results are presented here to show qualitatively the variation in shear stress between the outer and inner walls. Figure 17 compares the shear stress along the outer wall of planes A, C and E and figure 18 compares the values along the inner wall. As seen in these figures, the major difference in the shear-stress distribution between the outer and inner walls is the reversal in the direction of the shear along the inner wall, obviously due to the flow reversal during the diastolic duration. In both cases, the shear stress at plane A is slightly higher than at plane E, and this is due to the thickening of the boundary layer by the downstream end of the tube. It can also be observed that the magnitude of the shear stress is smaller at plane C compared with planes A and E. This is again due to the effect of secondary flows in flattening out the axial flow profiles between planes A and C and once again the profile being skewed towards the outer end of plane E. The shear-stress distributions at the top and bottom walls were qualitatively similar to that seen for the outer wall (figure 17) and are not shown here.

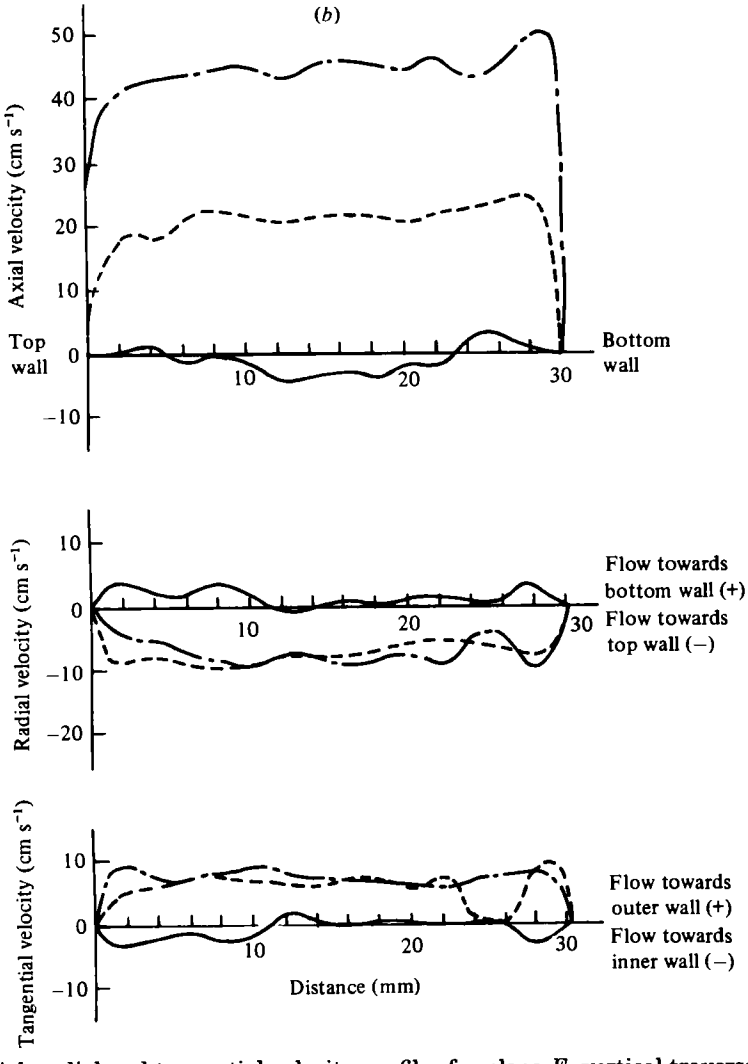

FIGURE 12. Axial, radial and tangential velocity profiles for plane E, vertical traverse. (a) ——, $J = 2$; – – –, $J = 6$; —·—, $J = 10$. (b) ——, $J = 17$; – – –, $J = 18$; —·—, $J = 19$.

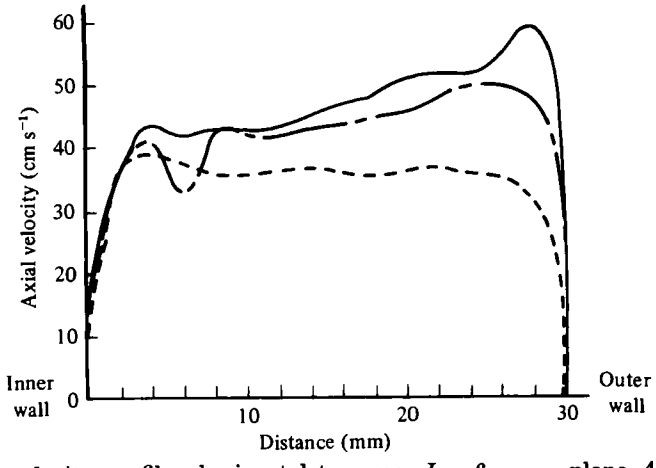

FIGURE 13. Axial velocity profiles, horizontal traverse, $J = 6$. ——, plane A; – – –, plane C; —·—, plane E.

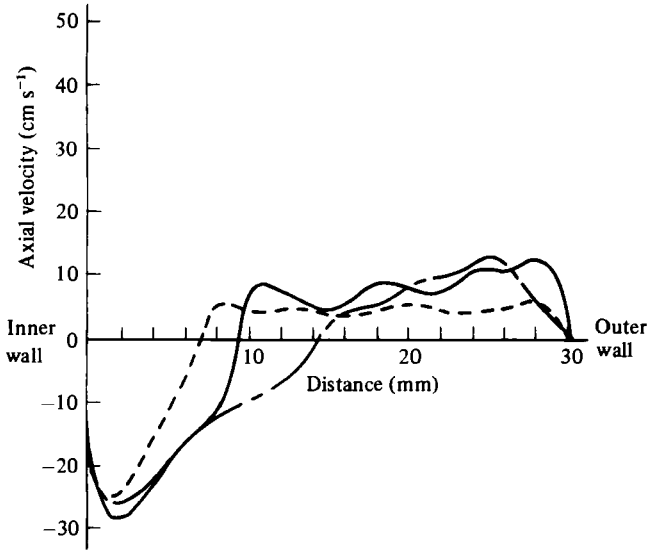

FIGURE 14. Axial velocity profiles, horizontal traverse, $J = 10$. ——, plane A; – – –, plane C; — · —, plane E.

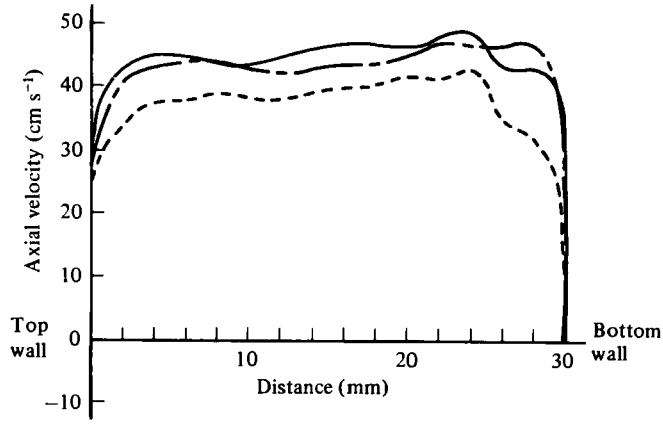

FIGURE 15. Axial velocity profiles, vertical traverse, $J = 6$. ——, plane A; – – –, plane C; — · —, plane E.

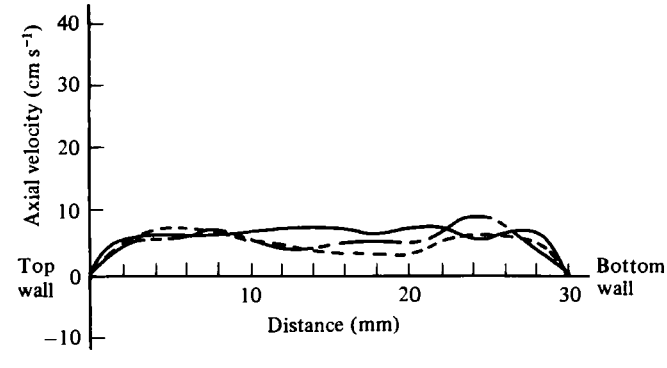

FIGURE 16. Axial velocity profiles, vertical traverse, $J = 10$. ——, plane A; – – –, plane C; — · —; plane E.

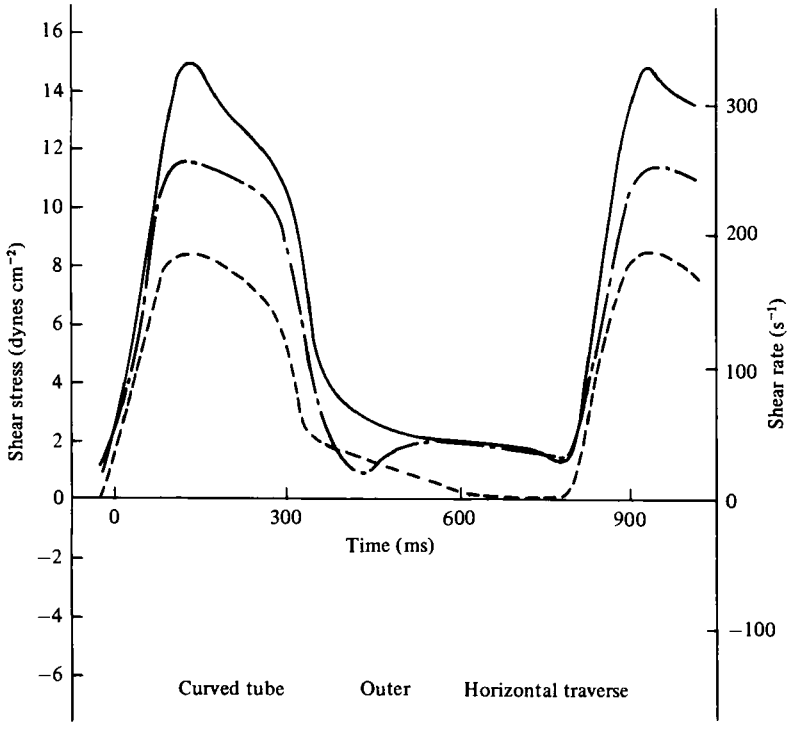

FIGURE 17. Variation with shear stress/rate with time at the outer wall of the curved tube. ——, plane A; – – –, plane C; —·—, plane E.

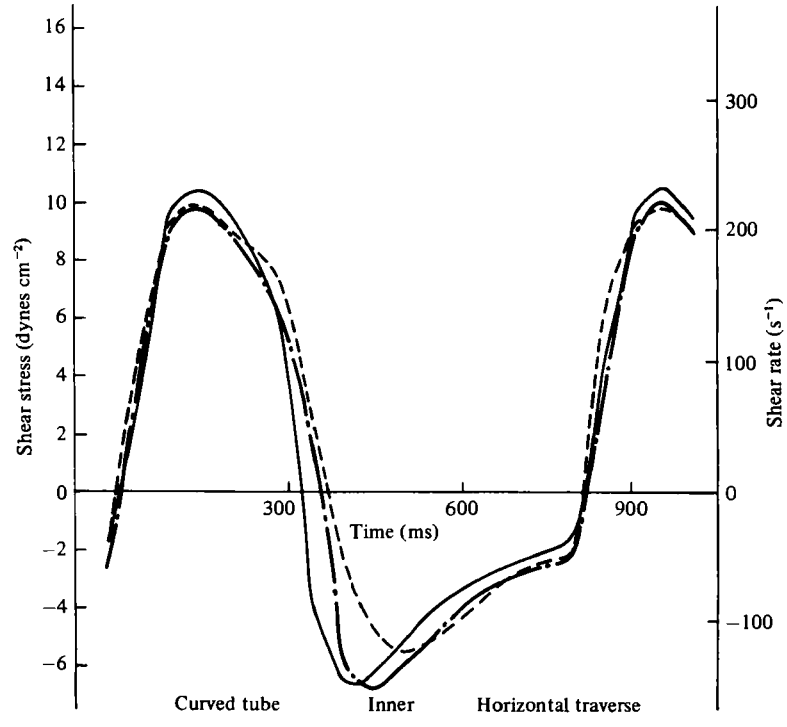

FIGURE 18. Variation in shear stress/rate with time at the inner wall of the curved tube. ——, plane A; – – –, plane C; —·—, plane E.

4. Conclusions

In summary, four features of pulsatile flow development in the curved tube should be observed. First is the presence of a strong reversed flow along the inner wall. This reversed flow is the result of an adverse pressure gradient generated by flow over a curved surface. It begins at the start of diastole, simultaneously with valve closure, and is progressively stronger as one moves downstream towards the tube exit. Over the course of diastole, it extends out into the central region of the tube and is most extensive at plane E compared to other planes in the upstream end. It is the presence of this region of reversed flow that determines the nature of the flow field during systole. Second is that the flow is not fully developed throughout the entire length of the curved tube. The flow of fluid in the core region is dramatically influenced by the nature of the flows within the boundary layer, as is characteristic of developing flows in entrance regions of curved pipes and tubes (Agrawal *et al.* 1978). Third is the vacillation of the peak axial velocity across the horizontal diameter of the tube from plane A to plane E. At plane A, the maximum is nearest the outer wall, more as a result of the flow reversal near the inner wall during diastole than because of centrifugal forces. At plane B, the axial velocity profile has shifted away from the outer wall resulting in a flat or blunt profile. At plane C, however, the peak axial flow is found near the inner wall and circumferential flows towards the inner wall can be measured across the vertical diameter of the tube. Plane D is a transitional stage in which the axial flow profile is seen to be the lowest at the centre of the tube. By plane E, the maximum is again found at the outer wall. Finally, trapped vortical motions are seen to occur at the inner wall of the tube at plane E, having originated as rotational motions in the boundary layer as a result of circumferential flows towards the inner wall in the regions of plane B and C, where the initial shift in axial momentum is first observed.

Stewartson, Cebeci & Chang (1980) have recently presented a numerical analysis of steady flow through a curved duct at large values of Dean number and they show that the boundary layer, generated at the entrance develop a collision structure in the neighbourhood of the inner wall after evolving for a finite distance down the duct. The entry condition to their solution procedure was an inviscid flow profile in a curved tube and they show that the boundary layer which develops at the outer wall of the tube spreads around to the inner wall in two directions. Their computations show that the boundary layers collide at a finite distance downstream from the entrance and they presume that a jet is set up directed towards the outer bend which eventually completes the circuit of the boundary layers. These observations seem to be at variance from the conclusions drawn from the experimental study presented here suggesting that the boundary layers which are generated at the outer wall travel in both directions and meet at the inner wall where trapped vortices are formed. The steady-flow dye studies of Scarton *et al.* (1977) also show that the fluid at the inner-wall boundary layer is trapped and does not re-enter into the core region. Even though Stewartson *et al.* (1980) point out that the experimental works of Agrawal *et al.* (1978) and Choi *et al.* (1979) tend to support their findings, further experiments are necessary to investigate the nature of the flow at the inner-wall boundary layer.

The results presented in this paper indicate *qualitatively* the nature of the flow in the human aortic arch. It is qualitative for several reasons. The flow chamber used in this study had a radius to radius-of-curvature ratio of 0·1 and the cross-section

is circular. However, the human aortic arch goemetry is irregular with a radius to radius-of-curvature ratio of about 0·4 in the primary bend. Moreover, the cross-section of the aorta is approximately elliptical and tapered so that the cross-sectional area reduces by about 45% between the ascending and descending portions. There are also three major arteries branching out at the top of the arch. The entry flow at the upstream of the aorta is affected by the aortic valve leaflets and the sinuses. All these complications have been avoided in the present study in order to delineate the effect of curvature on pulsatile flow. However, the pressure pulses in the left-ventricular and the curved-tube chambers as well as the flow rate have been adjusted to closely resemble the physiological situation.

It is interesting to note that larger incidence of atherosclerosis in the human aortic arch is observed towards the inner wall of the bend towards the descending section of the arch. In the light of the results presented in this study, it is also precisely the region where trapped vortical motions are observed. Moreover, a well-defined reversed flow is also observed along the inner wall throughout the diastolic region. Since the study reported in this paper, we have also completed the experiments on a model of the human aortic arch. Even in the arch model, we observed trapped vortices and reversed flow along the inner wall. However, the reversed flow in the arch diffused more into the cross-section of the tube and was not sustained throughout the cycle due to the acute curvatures encountered. The effect of these vortical motions and the directional changes in the wall shear along the inner wall on the endothelial lining may yield valuable information about the causes of this diseased state.

Partial support from National Heart, Lung and Blood Institute (NIH GRANT no. HL18156) is gratefully acknowledged. The authors wish to thank the Graduate College of The University of Iowa for providing the computer time and Shell Oil Company for providing glycerine.

REFERENCES

AGRAWAL, Y. C., TALBOT, L. & GONG, K. 1978 Laser anemometer study of flow development in curved circular pipes. *J. Fluid Mech.* **85**, 497–518.

BARUA, S. N. 1963 On secondary flow in stationary curved pipes. *Quart. J. Mech. Appl. Math.* **16**, 61–77.

BERGEL, D. H., NEREM, R. M. & SCHWARTZ, C. J. 1976 Fluid dynamic aspects of arterial disease. *Atherosclerosis* **23**, 253–261.

BOUSSINESQ, M. J. 1872 Infl. d. forces centrifuges sur le mouv. perm. varie de l'eau dans les canuz larges. *Paris, Soc. Philom. Bull.* **8**(6), 77–82.

CHANDRAN, K. B., HOSEY, R. R., GHISTA, D. N. & VAYO, V. W. 1979 Analysis of fully developed unsteady viscous flow in a curved elastic tube model to provide fluid mechanical data for some circulatory path-physiological situations and assist devices. *J. Biomech. Engng* **101**, 114–123.

CHANDRAN, K. B., SWANSON, W. M., GHISTA, D. N. & VAYO, H. W. 1974 Oscillatory flow in thin-walled curved elastic tubes. *Ann. Biomed. Engng* **2**, 392–412.

CHANDRAN, K. B., YEARWOOD, T. L. & WIETING, D. W. 1979 An experimental study of pulsatile flow in a curved tube. *J. Biomech.* **12**, 793–805.

CHOI, V. S., TALBOT, L. & CORNET, I. 1979 Experimental study of wall shear rates in the entry region of a curved tube. *J. Fluid Mech.* **93**, 229–274.

COLLINS, W. M. & DENNIS, S. C. R. 1975 The steady motion of a viscous fluid in a curved tube. *Quart. J. Mech. Appl. Math.* **28**, 133–156.

DEAN, W. R. 1927 Note on the motion of fluid in a curved pipe. *Phil. Mag.* **20**(7), 208–223.

DEAN, W. R. 1928 The streamline motion of fluid in a curved pipe. *Phil. Mag.* **30**(7), 673–693.

EUSTICE, J. 1911 Experiments on streamline motion in curved pipes. *Proc. Roy. Soc.* A **85**, 119–131.

GREENSPAN, A. D. 1973 Secondary flow in a curved tube. *J. Fluid Mech.* **57**, 167–176.

ITO, H. 1969 Laminar flow in curved pipes. *Z. angew. Math. Mech.* **49**, 653–663.

LYNE, W. H. 1971 Unsteady viscous flow in a curved pipe. *J. Fluid Mech.* **45**, 13–31.

MCCONALOGUE, D. J. & SRIVASTAVA, R. S. 1968 Motion of a fluid in a curved pipe. *Proc. Roy. Soc.* A **307**, 37–53.

MORGAN, G. W. & KIELY, J. P. 1954 Wave propagation in a viscous liquid contained in a flexible tube. *J. Acoust. Soc. Am.* **26**, 323–328.

MORI, Y. & NAKAYAMA, W. 1965 Study on forced convective heat transfer in curved pipes. First report. Laminar region. *Int. J. Heat Mass Transfer* **8**, 67–82.

MUNSON, B. R. 1975 Experimental results for oscillating flow in a curved pipe. *Phys. Fluids* **18**, 1607–1609.

OLSON, D. E. 1971 Fluid mechanics relevant to respiratory flow with curved elliptic tubes and bifurcating systems. Ph.D. thesis, Imperial College, London, England.

PATANKAR, S. V., PRATAP, V. S. & SPALDING, D. B. 1974 Prediction of laminar flow and heat transfer in helically coiled pipes. *J. Fluid Mech.* **62**, 539–551.

PEDLEY, T. J. 1974 Flow in the entrance of the aorta. *Fluid Dynamics of Arterial Disease* (ed. R. M. Nerem), Proc. of a Specialists' Meeting at Ohio State University, Columbus, Ohio.

PEDLEY, T. J. 1975 A thermal boundary layer in a reversing flow. *J. Fluid Mech.* **67**, 209–225.

PEDLEY, T. J. 1976 Viscous boundary layer in reversing flow. *J. Fluid Mech.* **74**, 59–79.

SANKARAIAH, M. & RAO, Y. V. N. 1973 Analysis of steady laminar flow of an incompressible Newtonian fluid through curved pipes of small curvature. *Trans. A.S.M.E.* I, *J. Fluid Engng* **95**, 75–80.

SCARTON, H. A., SHAH, P. M., & TSAPOGAS, M. J. 1977 Relationship of the spatial evolution of secondary flow in curved tubes to the aortic arch. *Mechanics in Engineering*, pp. 111–131. University of Waterloo Press.

SINGH, M. P. 1974 Entry flow in a curved pipe. *J. Fluid Mech.* **65**, 517–539.

SINGH, M. P., SINHA, P. C. & AGGARWAL, M. 1978 Flow in the entrance of the aorta. *J. Fluid Mech.* **87**, 97–120.

SMITH, F. T. 1975 Pulsatile flow in curved pipe. *J. Fluid Mech.* **71**, 417–539.

STEWARTSON, K., CEBECI, T. & CHANG, K. C. 1980 A boundary-layer collision in a curved duct. *Quart. J. Mech. Appl. Math.* **33**, 59–75.

THOMPSON, J. 1879 Flow round river bends. *Proc. Inst. Mech. Eng.* **2**, Plate 58, 456–460.

TRUESDELL, L. C. 1963 Numerical treatment of laminar flow through helical conduits. Ph.D. thesis, Case Institute of Technology.

WIETING, D. W. 1969 Dynamic flow characteristics of heart valves. Ph.D. dissertation, University of Texas, Austin.

YAO, L. S. & BERGER, S. A. 1975 Entry flow in a curved pipe. *J. Fluid Mech.* **67**, 177–196.

YEARWOOD, T. L. 1979 Steady and pulsatile flow analysis in a model of the human aortic arch. Ph.D. dissertation, Tulane University, New Orleans.

ZALOSH, R. G. & NELSON, W. G. 1973 Pulsating flow in a curved tube. *J. Fluid Mech.* **59**, 693–705.